A thermostat-consistent fully coupled molecular dynamics – generalised fluctuating hydrodynamics model

Xinjian Liu[a,b], Ivan Korotkin[c], Zhonghao Rao[a], Sergey Karabasov[b,*]

[a]School of Electrical and Power Engineering, China University of Mining and Technology, Xuzhou, 221116, China

[b]The School of Engineering and Materials Science, Queen Mary University of London, Mile End Road, E1 4NS London, United Kingdom

[c]Mathematical Sciences, University of Southampton, University Rd., SO17 1BJ, United Kingdom

*Corresponding author, s.karabasov@qmul.ac.uk

Abstract

The previously developed multiscale method for concurrently coupling atomistic and continuum hydrodynamic representations of the same chemical substance is extended to consistently incorporate the Langevin-type thermostat equations in the model. This allows not only to preserve the mass and momentum conservation laws based on the two-phase flow analogy modelling framework but also to capture the correct local fluctuations and temperature in the pure atomistic region of the hybrid model. Numerical results for the test problem of equilibrium isothermal fluctuations of SPC/E water are presented. Advantages of using local thermostat equations adjusted for the multi-resolution model for accurately capturing of the local water density in the atomistic part of the hybrid simulation domain are discussed. Comparisons with the reference pure all-atom molecular dynamics simulations in GROMACS show that the suggested hybrid models are by a factor of 5 to 20 faster depending on the simulation domain size.

1. Introduction

Hybrid multiscale methods, which resolve inter-atomic forces in the region of interest using Molecular Dynamics (MD) while representing the rest of the fluid by much more efficient Computational Fluid Dynamics (CFD) models, have a variety of use in many problems of science and engineering[1-4]. Multiscale approaches coupling MD and CFD methods can be cast into two broad categories, Domain Decomposition and Heterogeneous Multiscale Methods (DDM and HMM, respectively)[5-6].

HMM typically embeds a micro model described by an interaction potential between discrete particles in the nodes of a uniform Cartesian grid that covers the entire macroscopic simulation domain where Navier-Stokes (NS) equations are solved. The same approach can also be extended if the MD part of the model does not coincide with a grid node of the CFD solver, which is known as Internal-Flow Multiscale Method (IMM)[7]. Within the HMM approach, a macroscopic solution can be used to enforce a prescribed

strain rate or a mass flux at the boundaries of the microscopic model. The stresses obtained by averaging of the MD solution are then fed back to the macroscopic equations.

The DDM approach for coupling of MD equations with CFD was pioneered by O'Connell and Thompson[8] who coupled MD simulations with the solution of the Stokes equations. Further investigations along the same line of thought used Landau and Lifshitz Fluctuating Hydrodynamics (LL-FH) Navier Stokes model[9], which includes not only the simple time means but also statistical variances of thermal density and velocity fluctuations[10-12]. Depending on how the exchange between the MD and CFD regions is implemented, DDM approaches can be further classed into flux coupling and state coupling schemes. In flux coupling schemes, the momentum and mass fluxes of the non-overlapping MD and CFD regions are exchanged via a boundary condition at the interface to preserve the corresponding conservation laws[13-14]. In comparison with this, state coupling schemes use a finite overlap region to transfer the mass and momenta between the MD and CFD zones[15]. The finite overlap region allows for a smooth transition between the continuum and atomistic parts of the model. The coupling may also be improved by incorporating multi-resolution discrete particle models – from atomistic to coarse-grained particles[16-17]. Such refined formulations can be used to obtain sophisticated triple-scale (micro-meso-macro) models where multi-resolution particles are coupled with continuum flow models[17-18].

The current work follows the hybrid modelling approach developed in Ref.[19] and [20]. In this state-variable coupling-type method, the macroscopic and the microscopic parts of the model are regarded as two nominal "phases" of the same chemical substance. The interaction of the two phases is formulated as the conservation laws of mass and momenta. One phase stands for a continuum flow- and the other phase stands for a discrete atomistic phase- representation of the same liquid. The concentration of the atomistic phase is a user-defined function that defines the multiscale model resolution. The continuum phase is governed by the Landau and Lifshitz Fluctuating Hydrodynamics-type equations. In order to avoid any artificial phase separation, forcing terms are introduced in the MD particle equations, which are also included in the continuum flow equations of the model in order to preserve the conservation of mass and momentum. In Ref.[21] and [22], a simplified one-way coupled version of the original method was considered, which accounts for the continuum flow effect on microscopic particles without the feedback. When implemented in GROMACS[23], the approach was found to be sufficiently accurate for modelling of

a range of problems such as biomolecule diffusion[24], oscillations of a PCV2 virus capsid in water in equilibrium conditions[25], and the interaction of nano-confined water with material surfaces of an Atomic Force Microscope[26]. The one-way coupled model can be further refined by coupling it with multi-resolution particles in the framework of the AdResS method[27].

On the other hand, the full computational efficiency of the hybrid multiscale scheme can only be achieved when the complete two-way coupled scheme is implemented. Most consistently, the two-way coupled method was implemented by rearranging the governing equations of the two-phase flow analogy method into the so-called Generalised Landau-Lifshitz Fluctuating Hydrodynamics equations (GLL-FH)[28]. In comparison with the standard Fluctuating Hydrodynamics (FH) model, which is a statistical representation of molecular liquids at mesoscale, the GLL-FH equations reduce to the FH model at mesoscale but also exactly converge to control-volume averaged MD fields at microscale.

In the previous publications, fully coupled two-phase analogy model has been implemented first for an idealised 2D Mercedes-Benz water model[29] and then for a 3D liquid argon in GROMACS at both equilibrium and the non-equilibrium conditions[28]. Importantly, in each of the previous implementations an external MD thermostat was used to enforce the correct global temperature on MD particles and which effect was not consistently accounted for in the continuum part of the same model. Hence, the goal of the present article is to extend the hybrid MD-FH method to incorporate thermostat equations in both the MD particles' and the continuum field' part of the model. On the way, we will also investigate the importance of using a local thermostat model, which in comparison with the constant thermostat can be adjusted to the local resolution of the multiscale model.

2. Computational Method

2.1 Two-phase analogy equations

In the framework of the hybrid continuum-atomistic model[19], the computational domain is decomposed into three zones: a pure molecular dynamics particle zone (MD), a pure fluctuating hydrodynamics continuum zone (FH) and a hybrid continuum-particle region (MD-FH). A nominally two-phase fluid is considered. A user-defined concentration function, s is introduced that determines the model resolution – from atomistic ($s = 0$) to continuum ($s = 1$). In the intermediate MD-FH region the model

resolution smoothly varies, $0 < s < 1$. MD particle equations are solved in both the purely atomistic and the intermediate region. Continuum field equations are solved throughout the entire computational domain including the pure hydrodynamics region (s = 1). For numerical solution, the entire domain is covered by a Eulerian computational grid. Assuming an isothermal and electrically neutral flow process, the mass and momentum equations are decoupled from energy[11], and, following the standard two-phase modelling approach[30], the conservation laws of the continuum and particle phases are as follows:

for mass,

$$\delta_t\left(sm\right)+\sum_{\gamma=1}^{6}\left(s\rho\tilde{\mathbf{u}}\cdot d\mathbf{n}^{\gamma}\right)\cdot\delta t = J_1\cdot\delta t \tag{1}$$

$$\delta_t\left(\sum_{p=1}^{N}\left[\left(1-s_p\right)m_p\right]\right)+\sum_{\gamma=1}^{6}\left(\sum_{p=1}^{N_\gamma}\left[\left(1-s_p\right)\rho_p\mathbf{u}_p\right]\cdot d\mathbf{n}^{\gamma}\right)\cdot\delta t = -J_1\cdot\delta t \tag{2}$$

and for momenta:

$$\delta_t\left(smu_i\right)+\sum_{\gamma=1}^{6}\left(s\rho u_i\tilde{\mathbf{u}}\cdot d\mathbf{n}^{\gamma}\right)\cdot\delta t = sF_i\cdot V\delta t + J_2\cdot\delta t \tag{3}$$

$$\delta_t\left(\sum_{p=1}^{N}\left[\left(1-s_p\right)m_p u_{ip}\right]\right)+\sum_{\gamma=1}^{6}\left(\sum_{p=1}^{N_\gamma}\left[\left(1-s_p\right)\rho_p u_{ip}\mathbf{u}_p\right]\cdot d\mathbf{n}^{\gamma}\right)\cdot\delta t = \sum_{p=1}^{N}\left[\left(1-s_p\right)F_{ip}^{MD}\right]\cdot V\delta t - J_2\cdot\delta t\,. \tag{4}$$

Here i=1, 2, 3 denotes x, y and z components, variables with sub-index p correspond to particle phase while the continuum cell-volume and cell-flux averaged values do not contain the particle sub-index. γ corresponds to one of the six faces of the hexahedral control volume of the computational grid, V. m and ρ are the local mass and density of the continuum phase per given control volume. m_p and $\rho_p = m_p/V$ are the particle mass and its effective density per control volume, respectively. $\mathbf{u}_p$ and $\tilde{\mathbf{u}}$ correspond to particle velocity and velocity of the two phase 'mixture', which is given by $\tilde{u}_i = \left[s\rho u_i + \sum_{p=1}^{N}\left[\left(1-s_p\right)\rho_p u_{ip}\right]\right]\Big/\tilde{\rho}$. The mixture density is defined as $\tilde{\rho} = s\rho + \left(1-s\right)\sum_{p=1}^{N}\rho_p$. N is the number of particles per cell volume and N_γ denotes the number of particles crossing the cell face in the direction of the area normal $d\mathbf{n}^{\gamma}$, δt represents the change of each quantity over one time step. F_{ip}^{MD} refers

to the MD particle force exerted on each particle. The continuum force, $F_i = \nabla_j(\bar{\Pi}_{ij} + \tilde{\Pi}_{ij})$ includes both the deterministic and stochastic continuum Reynolds stress forces in accordance with the Landau-Lifshitz Fluctuating Hydrodynamic model[9]:

$$\begin{aligned}\bar{\Pi}_{ij} &= -(p - \zeta div\ \mathbf{u})\delta_{ij} + \eta(\partial_i u_j + \partial_j u_i - 2D^{-1} div\ \mathbf{u}\delta_{ij}) \\ \tilde{\Pi}_{ij} &= \zeta div\ \mathbf{u}\delta_{ij} + \eta(\partial_i \tilde{u}_j + \partial_j \tilde{u}_i - 2D^{-1} div\ \tilde{\mathbf{u}}\delta_{ij})\end{aligned} \tag{5}$$

wherein *i*, *j* = 1,2,3, are the spatial coordinates *x*, *y* and *z*. ζ and η are the shear and bulk viscosity coefficients, respectively. *D* is the dimension of the system and δ_{ij} is the Kronecker delta function. $\tilde{\Pi}_{ij}$ is a random Gaussian matrix with zero mean and covariance

$$\left\langle \tilde{\Pi}_{ij}(\mathbf{r}_1, t_1)\tilde{\Pi}_{kl}(\mathbf{r}_2, t_2) \right\rangle = 2k_B T[\eta(\delta_{ik}\delta_{jl} + \delta_{il}\delta_{jk}) + (\zeta - 2\mathrm{D}^{-1}\eta)\delta_{ij}\delta_{kl}] \times \delta(t_1 - t_2)\delta(\mathbf{r}_1 - \mathbf{r}_2) \tag{6}$$

For computational purposes, the stochastic stress tensor $\tilde{\Pi}_{ij}$ is represented explicitly by

$$\tilde{\Pi}_{ij} = \sqrt{\frac{2k_B T}{\Delta t_{FH} V}}(\sqrt{2}\sqrt{\eta} \cdot G_{ij}^S + \sqrt{D}\sqrt{\zeta} \cdot tr[\mathbf{G}] \cdot E_{ij}/D) \tag{7}$$

where $\mathbf{G}$ is a random Gaussian matrix with zero mean and covariance $\left\langle G_{ij} G_{kl} \right\rangle = \delta_{ij}\delta_{kl}$, $G_{ij}^s = \frac{G_{ij} + G_{ij}^T}{2} - tr[\mathbf{G}] \cdot E_{ij}/D$ is a random symmetric matrix with zero trace, $\mathbf{E}$ is the identity matrix with the components E_{ij}, $tr[\mathbf{G}]$ is the trace of the matrix $\mathbf{G}$, k_B is the Boltzmann constant, and Δt_{FH} is the continuum hydrodynamics integration time step. T is the thermodynamic temperature, which is equal to the target MD temperature T_0. For isothermal processes of interest in this work, a suitable isothermal equation of state (EoS), $p = p(\rho, T_0)$ is used which relates thermodynamic pressure and density of the continuum phase. Parameters of EoS are calibrated from a separate all-atom MD simulation.

The hybrid model is closed by specifying the source and sink terms, J_1 and J_2 in the mass and momentum equations. These terms are the effective forcing functions, which need to be calibrated appropriately. The terms depend on the user-defined phase concentration function *s* and serve to prevent the solution of the nominally two-phase fluid from artificial phase separations. These functions are defined

so that the residuals corresponding to the differences of the cell-averaged particle density and momenta from the same of the two-phase mixture , $\tilde{\rho} - \sum_{p=1}^{N} \rho_p$ and $\tilde{\rho}\tilde{u}_i - \sum_{p=1}^{N} \rho_p u_{ip}$ are driven to zero.

Notably, neither calibration of the J_1 and J_2 functions, nor the definition of the phase concentration function *s*, affect the total conservation laws of mass and momenta, which are governed by equations (1)-(4) where the sources and sinks of the two phases cancel out in the mixture mass and momenta [28].

2.2 Generalised Landau-Lifshitz model

The modified MD coordinate and velocity equations are defined by adding the relevant forcing terms to the pure MD equations, $\frac{dx_{ip}}{dt} = u_{ip}$, $\frac{du_{jp}}{dt} = F_{jp}(\mathbf{x}_p)$:

$$\frac{dx_{ip}}{dt} = (1-s_p)u_{ip} + s_p\tilde{u}_{ip} + \alpha s_p(1-s_p)\frac{\partial \rho'}{\partial x_i}\Big/\sum_{p=1}^{N}\rho_p \tag{8}$$

and

$$\frac{du_{jp}}{dt} = (1-s_p)F_{jp}^{MD}\Big/\rho_p + s_p F_{jp}\Big/\sum_{p=1}^{N}\rho_p + \left[\frac{\partial}{\partial x_i}\left(\frac{\sum_{p=1}^{N}\left[\alpha s_p\left(1-s_p\right)u_{jp}\rho_p\frac{\partial \rho'}{\partial x_i}\right]}{\sum_{p=1}^{N}\rho_p}\right)\right]_p\Big/\sum_{p=1}^{N}\rho_p + \left[\beta s\left(1-s\right)q_j'\right]_p\Big/\sum_{p=1}^{N}\rho_p \tag{9}$$

where *i*, *j* = 1,2,3 are Cartesian coordinate components, $\rho' = \tilde{\rho} - \sum_{p=1}^{N}\rho_p$ and $q_i' = \tilde{\rho}\tilde{u}_i - \sum_{p=1}^{N}\rho_p u_{ip}$, *p* is the particle sub-index which refers to the value defined or interpolated to the particle location, and $\alpha, \beta > 0$ are the adjustable constants which need to be obtained from the model calibration.

Forcing terms on the right-hand side include control-volume-averaged gradient ∇f , which is computed in accordance with the Gauss-Ostrogradski (Divergence) theorem, $\frac{\sum_{\gamma=1,6} f d\mathbf{n}^{\gamma}}{V}$. The same compact notation will be used in further places of the article.

The source/sink terms J_1 and J_2 in (1)-(4) are implicitly defined by specifying the equations for mass and momentum residuals. The latter are driven to zero using the convection-diffusion-reaction type equation,

$$\frac{\delta_t \rho'}{\delta t} + \frac{1}{V}\sum_{\gamma=1}^{6}\left(\rho' \tilde{u}_i \cdot dn_i^{\gamma}\right) = \alpha \frac{1}{V}\sum_{\gamma=1}^{6} s(1-s)\frac{\partial \rho'}{\partial x_i} dn_i^{\gamma} \tag{10}$$

$$\frac{\delta_t q_i'}{\delta t} + \frac{1}{V}\sum_{\gamma=1}^{6}\left(q_i' \tilde{u}_j \cdot dn_j^{\gamma}\right) = -\beta s(1-s)\left(\tilde{\rho}\tilde{u}_i - \sum_{p=1}^{N}\rho_p u_{ip}\right), \; i, j = 1, 2, 3 \tag{11}$$

Following Ref.[28] , by substituting the modified MD equations (8) and (9) in the following conservation laws of mass and momenta of MD particles,

$$\frac{\delta_t\left(\sum_{p=1}^{N} m_p\right)}{\delta t} + \sum_{\gamma=1}^{6}\left[\left(\sum_{p=1}^{N_\gamma}\frac{d\mathbf{x}_p}{dt}\rho_p\right)d\mathbf{n}^{\gamma}\right] = 0 \text{ and} \tag{12}$$

$$\delta_t\left(\sum_{p=1}^{N} m_p u_{ip}\right) + \sum_{\gamma=1}^{6}\left[\left(\sum_{p=1}^{N_\gamma}\frac{d\mathbf{x}_p}{dt}\rho_p u_{ip}\right)d\mathbf{n}^{\gamma}\right]\cdot\delta t = \sum_{p=1}^{N}\left[m_p\frac{du_{ip}}{dt}\right]\cdot\delta t\,, \tag{13}$$

after some re-arrangement and introducing the dependent variables $\rho^* = \tilde{\rho} - \rho'$ and $q_i = \tilde{u}_i\tilde{\rho} - q_i'$, the so-called Generalised Landau-Lifshitz Fluctuating Hydrodynamics (GLL-FH) equations are obtained

$$\frac{\delta_t \rho^*}{\delta t} + \frac{1}{V}\sum_{\gamma=1}^{6}\left[s\rho^*\tilde{u}_i \cdot dn_i^{\gamma}\right] = Q_\rho - \alpha\frac{1}{V}\sum_{\gamma=1}^{6} s(1-s)\frac{\partial\rho'}{\partial x_i}dn_i^{\gamma} \tag{14}$$

$$\frac{\delta_t q_i}{\delta t} + \frac{1}{V}\sum_{\gamma=1}^{6}\left[sq_i\tilde{u}_j \cdot dn_j^{\gamma}\right] = Q_i + sF_i + \beta s(1-s)\cdot q_i' \;\; i, j=1, 2, 3. \tag{15}$$

The right-hand-side terms of the above equations include the control averaged mass and momentum terms corresponding to the feedback from the MD particles to the continuum hydrodynamics phase,

$$Q_\rho = -\frac{1}{V}\sum_{\gamma=1}^{6}\left[\left(\sum_{p=1}^{N_\gamma}(1-s_p)u_{ip}\rho_p\right)dn_i^{\gamma}\right] \tag{16}$$

and

$$Q_i = \sum_{p=1}^{N}\left[(1-s_p)F_{ip}^{\;MD}\right] - \frac{1}{V}\sum_{\gamma=1}^{6}\left[\sum_{p=1}^{N_\gamma}\left((1-s_p)u_{jp}\rho_p u_{ip}\right)dn_j^{\gamma}\right] \; i, j=1, 2, 3. \tag{17}$$

The GLL-FH equations (10), (11), (14)-(17) are solved by the finite-volume method on a uniform computational grid with control volume V. The integration time step, Δt_{FH} is 10 times larger in comparison with the MD time step, Δt_{MD} as discussed in Ref.[28]. In the two-way coupled solution, the hydrodynamic fields are driven by the collective dynamics of MD particles while coordinates and velocities of the MD particles are concurrently updated in accordance with (8) and (9).

2.3 Langevin dissipation in MD particle equations and its effect on the conservation laws

The modified MD particle equations are solved by the standard Leapfrog algorithm[31] and using appropriate central finite-volume approximation for the continuum forcing terms for the MD particle coordinate,

$$\frac{x_{ip}\left(t+\Delta t_{MD}\right)-x_{ip}\left(t\right)}{\Delta t_{MD}}=(1-s_p)u_{ip}\left(t+\frac{1}{2}\Delta t_{MD}\right)+s_p\tilde{u}_{ip}^{\,n+1/2}+\alpha s_p(1-s_p)\frac{\partial\rho'^{n+1/2}}{\partial x_i}\Bigg/\sum_{p=1}^{N}\rho_p\left(t\right) \tag{18}$$

and velocity,

$$\frac{u_{jp}\left(t+\frac{1}{2}\Delta t_{MD}\right)-u_{jp}\left(t-\frac{1}{2}\Delta t_{MD}\right)}{\Delta t_{MD}}=(1-s_p)F_{jp}^{MD}\Big/\rho_p+s_pF_{jp}^{\,n+1/2}\Bigg/\sum_{p=1}^{N}\rho_p+$$
$$+\left[\frac{\partial}{\partial x_i}\left(\frac{\sum_{p=1}^{N}\left[\alpha s_p\left(1-s_p\right)u_{jp}\rho_p\left(t\right)\frac{\partial\rho'^{n+1/2}}{\partial x_i}\right]}{\sum_{p=1}^{N}\rho_p}\right)\right]_p\Bigg/\sum_{p=1}^{N}\rho_p\left(t\right)+\left[\beta s\left(1-s\right)q_j'^{\,n+1/2}\right]\Bigg/\sum_{p=1}^{N}\rho_p\left(t\right) \tag{19}$$

where, i, j = 1, 2, 3, Δt_{MD} is the MD time step, and superscript n stands for the time discretisation of the continuum flow equations (10), (11), (14)-(17).

In order to stabilise the time-integration of the particle equations (18), (19), one standard choice is to apply the Berendsen thermostat[32] at each MD time step so that the ensemble-averaged temperature of MD particles always satisfies the prescribed value of T_0=298.15 K. This is achieved by solving an additional dissipative equation for the MD particle velocity after the update step:

$$\frac{u_{i,p}^{\,final}\left(t+\frac{1}{2}\Delta t_{MD}\right)-u_{i,p}\left(t+\frac{1}{2}\Delta t_{MD}\right)}{\Delta t_{MD}}=-\frac{1-\lambda}{\Delta t_{MD\;i,p}}\left(t+\frac{1}{2}\Delta t_{MD}\right)\;i=1,2,3 \tag{20}$$

where $u_{i,p}^{final}$ is the finally updated velocity value at the new time level and the rescaling parameter is

$$\lambda = \sqrt{1 + \frac{\Delta t_{MD}}{\tau}\left(\frac{T_{ref}}{T} - 1\right)}. \tag{21}$$

In the above expression, τ is a characteristic relaxation time of the thermostat, and T_{ref} is the target MD temperature. T is the instantaneous temperature of MD particles for the relevant ensemble averaging that is directly related to the ensemble-averaged kinetic energy of MD particles in accordance with the equipartition.

$$T = \frac{1}{3Nk_B}\sum_{p=1}^{N} m_p \left|u_p\right|^2 \tag{21a}$$

where the sum is taken over the entire simulation domain.

The hybrid method described by equations (10), (11), (14)-(21), where the particle temperature is measured by averaging over the entire computational domain corresponds to the model considered in Ref.[28]. It will be further referred to as Global Thermostat model (GT).

In MD simulations, thermostat generates additional dissipation, which is added to the discrete particle system in order to counterbalance the increase of fluctuation energy occurring due to the numerical integration of the particle equations. The same can be achieved by incorporating the thermostat model directly in the modified MD particle momentum equations, and Eqs.(18), (19) become

$$\frac{dx_{ip}}{dt} = u_i^* \tag{22}$$

$$\frac{du_{ip}}{dt} = -\gamma u_{ip} + F_i^* \tag{23}$$

where $\gamma = \frac{1-\lambda}{\Delta t_{MD}}$, $u_i^* = \frac{dx_{ip}}{dt} = (1-s_p)u_{ip} + s_p\tilde{u}_{ip} + \alpha s_p(1-s_p)\frac{\partial \rho'}{\partial x_i}\Big/\sum_{p=1}^{N}\rho_p$,

and

$$F_j^* = (1-s_p)F_{jp}^{MD} \Big/ \rho_p + s_p F_{jp} \Big/ \sum_{p=1}^{N} \rho_p + \left[\frac{\partial}{\partial x_i} \left(\frac{\sum_{p=1}^{N} \left[\alpha s_p \left(1-s_p\right) u_{jp} \rho_p \frac{\partial \rho'}{\partial x_i} \right]}{\sum_{p=1}^{N} \rho_p} \right) \right] \Big/ \sum_{p=1}^{N} \rho_p$$

$$+ \left[\beta s \left(1-s\right) m_j' \right] \Big/ \sum_{p=1}^{N} \rho_p \qquad (24)$$

In turn, by substituting the modified MD velocity equations (23) into the particle momentum equation (13), and following the same steps outlined above, an additional dissipative source term appears in the momentum component of the continuum hydrodynamics equation (15),

$$Q_i = \sum_{p=1}^{N} \left[\left(1-s_p\right) F_{ip}^{MD} \right] - \frac{1}{V} \sum_{\gamma=1}^{6} \left[\sum_{p=1}^{N_\gamma} \left(\left(1-s_p\right) u_{jp} \rho_p u_{ip} \right) dn_j^\gamma \right] - \gamma \sum_{p=1}^{N} u_{ip} \rho_p \qquad (17a)$$

which can be compared with the original expression (17).

2.4 The new local thermostat consistent Langevin version of the hybrid MD-FH model

Following Ref.[27], Eq.(23) can be exactly integrated to

$$u_{ip}\left(t+\frac{\Delta t}{2}\right) = u_{ip}\left(t-\frac{\Delta t}{2}\right) \mathrm{e}^{-\gamma \Delta t} + \mathrm{e}^{-\gamma \Delta t} \int_{-\Delta t/2}^{\Delta t/2} \mathrm{e}^{-\gamma t'} F_i^*\left(t+t'\right) dt' \qquad (25)$$

Furthermore, by approximating $F_i^*\left(t'\right) \approx F_i^*\left(t+\Delta t\right)$ in Eq.(23), substituting the obtained expression for $u_{ip}\left(t+\Delta t\right)$ to the modified MD coordinate equation (23), and analytically evaluating the integrals in the coordinate and momentum equations with retaining only the leading order terms, the modified Leapfrog scheme is obtained,

$$x_{ip}\left(t+\Delta t\right) = x_{ip}\left(t\right) + u_i^* \frac{\mathrm{e}^{\gamma \Delta t}-1}{\gamma} \qquad (26)$$

$$u_{ip}\left(t+\frac{\Delta t}{2}\right) = u_{ip}\left(t-\frac{\Delta t}{2}\right) \mathrm{e}^{-\gamma \Delta t} + F_i^* \frac{\mathrm{e}^{-\gamma \Delta t/2} - \mathrm{e}^{-3\gamma \Delta t}}{\gamma}, \qquad (27)$$

which converges to the original Leapfrog method (18), (19) in the limiting case of deactivating the thermostat model $\gamma \to 0$.

The modified GLL-FH method based on equations (10), (11), (14)-(16), (17a), and (22)-(27), where the particle temperature is measured by averaging over the entire computational domain as in the previously considered GT model, will be further referred to as Langevin Constant Thermostat (LCT).

The next step is to further adjust the thermostat term to make it sensitive to the phase concentration parameter *s*, which determines the local resolution of the hybrid MD-FH model. Such adjustment may be needed since, for example, as discussed in the introduction, the kinetic energy of MD particles does not represent the true temperature of the two-phase mixture in the hybrid MD/FH domain where the continuum hydrodynamics effect on temperature is important. For instance, in the hydrodynamics-dominated region, where *s* tends 1, the 'coarse-grained' MD particles move with a characteristic velocity that is equal to the ensemble-averaged thermal velocity fluctuation in control volume V and with time step Δt_{FH}. However, because of the averaging, the ensemble-averaged velocity fluctuation is much smaller in comparison with the thermal velocity of individual atoms.

In the absence of a precise definition of temperature of the hybrid MD-FH system, the local thermostat model is adjusted by introducing a variable temperature function $T_{ref}(s)$ that is equal to the target MD temperature, T_0 = 298.15 K in the pure MD region and decreases with *s* increasing. In order to derive a suitable expression for $T_{ref}(s)$, let us consider a balance equation for enthalpy of the two-phase fluid corresponding to a mixture of the continuum hydrodynamics phase and the discrete MD phase which partially occupy the same control volume V,

$$\frac{1}{3Nk_B}\sum_{p=1}^{N}\rho_p V_p^{(\mathrm{eff})}\left|u_p\right|^2 + sT_0 = T_0 \tag{28}$$

Here the first term on the left-hand-side is the partial volume contribution of the discrete particle phase, the second term on the left-hand-side is the partial volume contribution of the continuum phase, and $\left|u_p\right|$ is the particle velocity magnitude. The thermodynamic temperature of the continuum phase is equal to the target temperature of the system.

$V_p^{(\mathrm{eff})} \le V$ is some effective partial volume occupied by each particle in control volume V, which needs to be defined. As *s* increases with coarsening the hybrid model resolution, MD particles become less

mobile thereby occupying a smaller part of the control volume. On the other hand, particle velocities contribute to the local temperature, which can be measured via the ensemble-averaged kinetic energy of the particles (21a). To close the model, the effective control volume $V_p^{(\mathrm{eff})}$ occupied by each particle can be related to the control volume V. For example, a simple-minded approach would be to assume that $V_p^{(\mathrm{eff})} = (1-s)V$ in accordance with the geometrical reduction of the effective volume of the MD particle phase as s increases in the hybrid MD-FH region. Substituting this definition of the effective volume to the enthalpy equation (28) will result in the previously considered LCT model, where the reference temperature $T_{ref}(s)$ is equal to T_0 for all s (see also Eq.(31)). However, because of the non-local particle-particle interactions and the particle inertia effect, it can be expected that MD particles do not strictly obey the geometrical law of the MD phase volume reduction as a function of s but remain mobile over a larger part of the volume,

$$V_p^{(\mathrm{eff})} = f(s), 1-s < f(s) < 1 \tag{29}$$

Numerical experiments (Appendix A) show that good choices for the shape function $f(s)$ include

$$f(s) = \sqrt{(1-s)} \tag{30a}$$

and

$$f(s) = (1-s/2) \tag{30b}$$

which correspond to the same leading term in the atomistic part of the hybrid simulation domain at $s<<1$. By combining Eq.(28) with (30a) (or (30b)) and using Eq.(21a) to express the volume averaged kinetic energy via the temperature, the final expression for the resolution-dependent reference temperature in the thermostat exponent Eq.(21) is given by

$$T_{ref} = \frac{1-s}{f(s)} T_0 \tag{31}$$

The s-dependent thermostat modification of the LCT model, where instead of $T_{ref}(s)$ equal to T_0 the above derived expression (31) is used will be further referred to as Local Langevin Thermostat model (LLT). In comparison with the previously considered GT and LCT models, the local thermostat is also based on measuring the particle temperature by averaging over each local control volume, V. In this

paper, all presented results corresponding to the local thermostat are based on the shape function defined by Eq.(30b).

2.5 The choice of the thermostat model

It can be noted that the constant dissipation term makes the particle momentum equation (23) similar to the stochastic thermostat of Brownian dynamics. Indeed, the forcing term F^* in Eq.(24) incorporates the fluctuating hydrodynamics force $\tilde{F}$, which corresponds to a gradient of the corresponding stochastic Reynolds stress $\tilde{\Pi}_{ij}$ (5), and which becomes partially balanced by the Langevin damping. However, in comparison with the stochastic thermostat model driven by Brownian dynamics[33], the stochastic hydrodynamic term of the suggested model is only active in the hybrid part of the domain ($s > 0$) while the Langevin damping vanishes in the particle-free part of the domain (see Eq.(17a)). Furthermore, the produced dissipation does not violate the total momentum conservation because of the two-phase flow analogy formulation, where the sources and the sinks of the two phases (equations (3) and (4)) cancel out for the mixture momentum, which corresponds to $\tilde{\rho} = s\rho + (1-s)\sum_{p=1}^{N} \rho_p$ and $\tilde{u}_i = \left[s\rho u_i + \sum_{p=1}^{N} \left[(1-s_p)\rho_p u_{ip} \right] \right] \Big/ \tilde{\rho}$. By the same virtue, the suggested approach is also different from other hybrid coupling schemes based on Langevin dynamics, for example, such as[34], where a Langevin damping term together with a random force term were added to the MD equations of motion between the pure atomistic and the continuum flow regions.

An important advantage of the Berendsen thermostat is simplicity. However, although this thermostat equilibrates the system to a desired temperature in the pure atomistic region ($s = 0$), it cannot generate a correct canonical ensemble unless a large molecular system is considered. Notably, the suggested modelling framework can be extended to the Nose-Hoover thermostat model[35] which is free from the above drawback. For example, one can consider replacing the dissipation exponent in Eq.(23), $\gamma = \frac{1-\lambda}{\Delta t_{MD}}$ by the Nose-Hoover evolutionary equation for $\gamma(t)$,

$$\frac{d\gamma}{dt} = \lambda \left[\sum_{p=1}^{N} \frac{m_p \left| u_p \right|^2}{2} - \frac{3N+1}{2} k_B T_{ref} \right] \tag{23a}$$

where $\lambda > 0$ corresponds to a friction coefficient.

At the equilibrium state, $\frac{d\gamma}{dt} = 0$ the kinetic energy is equal to $\frac{3N+1}{2} k_B T_{ref}$ as required by the equipartition, and wherein the additional degree of freedom in comparison with (21a) comes from γ.

The continuum equations of the model including (17a) will remain unaffected by Eq.(23a) but the Leapfrog scheme (18)-(20) will need to be modified accordingly, which modification will be the subject of future work.

3. Numerical example: thermostat consistent modelling of equilibrium fluctuations of water

3.1 Test problem

As a benchmark test case, isothermal water fluctuations in a cubical water volume at equilibrium conditions are considered. The problem configuration is similar to the one considered in Ref.[28] but instead of the idealised Lennard-Jones liquid, SPC/E water is used here.

Fig.1 shows the entire computational domain which includes a larger hydrodynamic box domain which overlaps with a smaller particle domain. Continuum flow equations are solved in the entire computational domain and the MD particle equations are solved in the inner particle domain based on NVT ensemble.

Two computational domains are considered, which correspond to 9×9×9 and 17×17×17 elementary control volumes, V. The two domains will be further referred to as the small and the large simulation boxes, respectively. Each elementary control volume is filled with 243 water molecules at the normal atmospheric pressure and room temperature conditions. The size of the MD particle box corresponds to 5×5×5 control volumes. Periodic boundary conditions are used for both the continuum and interior particle

domains. Outside the internal particle domain s is set to 1. Inside the particle domain, a spherically symmetric s-function is specified,

$$s(r)=\begin{cases} S_{\min}=0, & r \le R_{MD} \\ \dfrac{r-R_{MD}}{R_{FH}-R_{MD}}(S_{\max}-S_{\min})+S_{\min}, & R_{MD}<r<R_{FH} \\ S_{\max}, & r \ge R_{FH} \end{cases}, \tag{32}$$

which corresponds to the pure MD region in the centre and the hybrid continuum-atomistic region at the periphery of the particle box. Here r is the distance from the centre of the box, and R_{MD} and R_{FH} are the radii of the pure MD zone and the hybrid MD/FH zone in the particle domain. Values of these and other model parameters are obtained from a suitable calibration of the hybrid model. Table 1 provides a summary of the model parameters.

It can be noted that while the two-phase flow analogy modelling framework permits any shapes of the s-function including multiply-connected[26] and time-dependant regions[24], accuracy of the hybrid model remains generally sensitive to this function. Hence, in the current work, a simple spherical s-function is used.

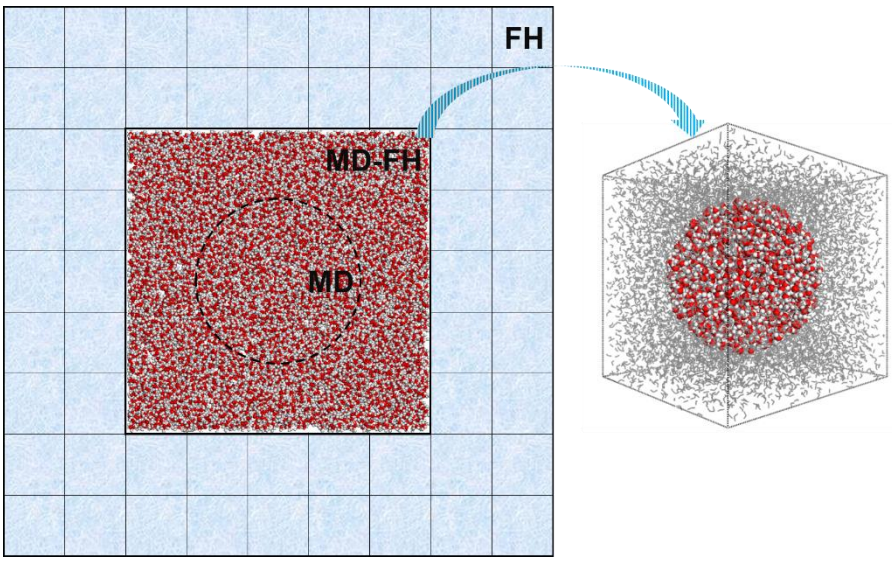

Fig. 1. Computational setup for the simulation of water fluctuations at equilibrium isothermal conditions: the overlapping continuum and particle box domains. Insert shows the outline of the spherical pure MD zone (s = 0) inside the particle box.

Table 1. Simulation parameters used in GROMACS for SPC/E water and the viscosity values used in the LL-FH code.

	LLT	LCT	GT

Number of atoms (molecules)	91125 (30375)		
Molecular mass ($g \cdot mol^{-1}$)	18.015		
Temperature (K)	298.15		
MD box volume (nm^3)	9.686×9.686×9.686		
MD time step (ps)	0.001		
Continuum solver time step (ps)	0.01		
Average density ($amu \cdot nm^{-3}$)	602.18		
Shear viscosity ($amu \cdot nm^{-1} \cdot ps^{-1}$)	409.496		
Bulk viscosity ($amu \cdot nm^{-1} \cdot ps^{-1}$)	933.41		
Maximum concentration of the hydrodynamic phase in the particle domain $s_{\max}$	0.5		
Number of control volumes in the MD box domain	5×5×5		
Number of control volumes in the continuum box domain	9×9×9&17×17×17	9×9×9&17×17×17	9×9×9&17×17×17
Dimensionless radius of the pure MD zone, $2R_{MD}V^{-1/3}$	0.5		
Dimensionless radius of the pure MD/FH zone, $2R_{FH}V^{-1/3}$	0.8		0.9
MD/FH coupling parameters, α ($nm^2 \cdot ps^{-1}$), β (ps^{-1})	100, 50		40, 40
Thermostat relaxation time, (ps)	0.36		0.1

3.2 Analysis of the model results

Tables 2a and b summarise results of the GT, LCT, and LLT models for the standard deviations of density and velocity fluctuations. Both the solutions of the MD particle and the continuum hydrodynamics phase of the models are shown. The fluctuations are ensemble-averaged over each control volume V of the entire 9×9×9 or 17×17×17 computational domains. Analytical solutions based on the grand-canonical ensemble fluctuating hydrodynamics theory are provided in each case, $STD(\rho) = c_T^{-1}\sqrt{\rho k_B \frac{T_0}{V}}$ and $STD(u) = \sqrt{k_B \frac{T_0}{\rho V}}$ for comparison, where c_T^{-1} is the isothermal speed of sound.

For each hybrid model solution (apart from the GT model in the small box which diverges), the standard deviations of the MD and the continuum hydrodynamics part of the multiscale model are very close. This confirms the absence of artificial phase separations thereby confirming that the coupling parameters of the model have been specified correctly.

The GT model is found to be extremely sensitive to the size of the hydrodynamic simulation domain. Its solution becomes stable for the large 17×17×17 domain, once the continuum hydrodynamics boundary is moved further away from the particle zone. However, the model still notably overestimates the standard deviations of the density and velocity fluctuations (Tables 2a and b) by 60-70% for both the MD particles and the continuum part of the solution.

The thermostat consistent LCT and the LLT water models are much more robust in comparison with GT. The accuracy of their solutions tends to improve as the hydrodynamics domain becomes larger, which can be good news for engineering applications where macroscopically large hydrodynamic domains are used. LCT captures the fluctuations particularly accurately (within 7-11% error for density and less than 2% error for velocities). In comparison with this, the error of the LLT model somewhat larger: it underestimates fluctuations by 18-26% for density and 18-20% for velocities. The lower fluctuations of LLT are explained by the fact that the local thermostat is designed to adjust to the particle-to-continuum resolution of the hybrid model, which reduces the reference particle temperature in the hydrodynamics dominated regions thereby reducing the ensemble-averaged fluctuation result over the entire system. What is most important in the simulations is to accurately capture fluctuations in the pure MD zone. Hence, Table 3 shows standard deviations of density and velocity fluctuations computed in control volume corresponding to the pure MD zone, s=0. In this case, the standard deviations are defined based on the fluctuation of the MD particle densities and velocities from the cell-averaged MD quantities, where the averaging is performed over the same pure MD control volume. In this case, comparisons with the statistical theory are problematic because of the small ensemble size. However, in comparison with the pure all-atom MD solutions the accuracy of the LLT model corresponds to less than 0.2% error for density and 11% for velocity fluctuations.

TABLE 2 (a). Standard deviations of the density in the MD-FH domain.

	STD_ρ_{MD} (amu·nm^{-3})	STD_ρ_{FH} (amu·nm^{-3})
GT (FH cells 17×17×17)	17.687	16.714
LCT (FH cells 9×9×9)	8.868	8.928
LCT	9.312	9.369

(FH cells 17×17×17)		
LLT (FH cells 9×9×9)	7.409	7.460
LLT (FH cells 17×17×17)	8.208	8.254
Analytical solution	10.049	

TABLE 2 (b). Standard deviations of the velocity fluctuations in the MD-FH domain.

	$STD\_u_{x\_MD}$ (nm·ps^{-1})	$STD\_u_{y\_MD}$ (nm·ps^{-1})	$STD\_u_{z\_MD}$ (nm·ps^{-1})	$STD\_u_{x\_FH}$ (nm·ps^{-1})	$STD\_u_{y\_FH}$ (nm·ps^{-1})	$STD\_u_{z\_FH}$ (nm·ps^{-1})
GT (FH cells 17×17×17)	0.0314	0.0314	0.0312	0.0305	0.0309	0.0315
LCT (FH cells 9×9×9)	0.0239	0.0238	0.0234	0.0243	0.0241	0.0238
LCT (FH cells 17×17×17)	0.0234	0.0235	0.0234	0.0238	0.0239	0.0238
LLT (FH cells 9×9×9)	0.0198	0.0197	0.0197	0.0200	0.0201	0.0199
LLT (FH cells 17×17×17)	0.0197	0.0197	0.0197	0.0200	0.0200	0.0203
Analytical solution	0.0238					

TABLE 3 (a). Standard deviations of the effective particle density in the pure MD domain.

	STD_ρ (amu·nm^{-3})
LLT	0.9707
Pure MD	0.9718

TABLE 3 (b). Standard deviations of the particle velocity fluctuations in the pure MD domain.

	STD_u_x (nm·ps^{-1})	STD_u_y (nm·ps^{-1})	STD_u_z (nm·ps^{-1})
LLT	0.8687	0.8671	0.8675
Pure MD	0.9678	0.9664	0.9567

Fig.2 shows cell-averaged density and temperature computed in the pure MD zone for all three models, GT, LCT and LLT. For LCT and LLT, the solutions for two domain sizes, 9×9×9 and 17×17×17 are presented.

Consistently with the previously reported results of the GT model for fluctuations, it predicts a much higher temperature and a lower density in the pure MD zone. In contrast to this, both the LCT and the LLT models capture the local temperature in the MD zone quite well. Furthermore, the LCT solution

overestimates the cell-averaged water density by 12% while the LLT error for the same quantity is within 4%. Recalling that water is a highly incompressible substance, the reduced error in density suggests that the LLT model is also much more accurate in preserving the reference pressure locally in comparison with the LCT model.

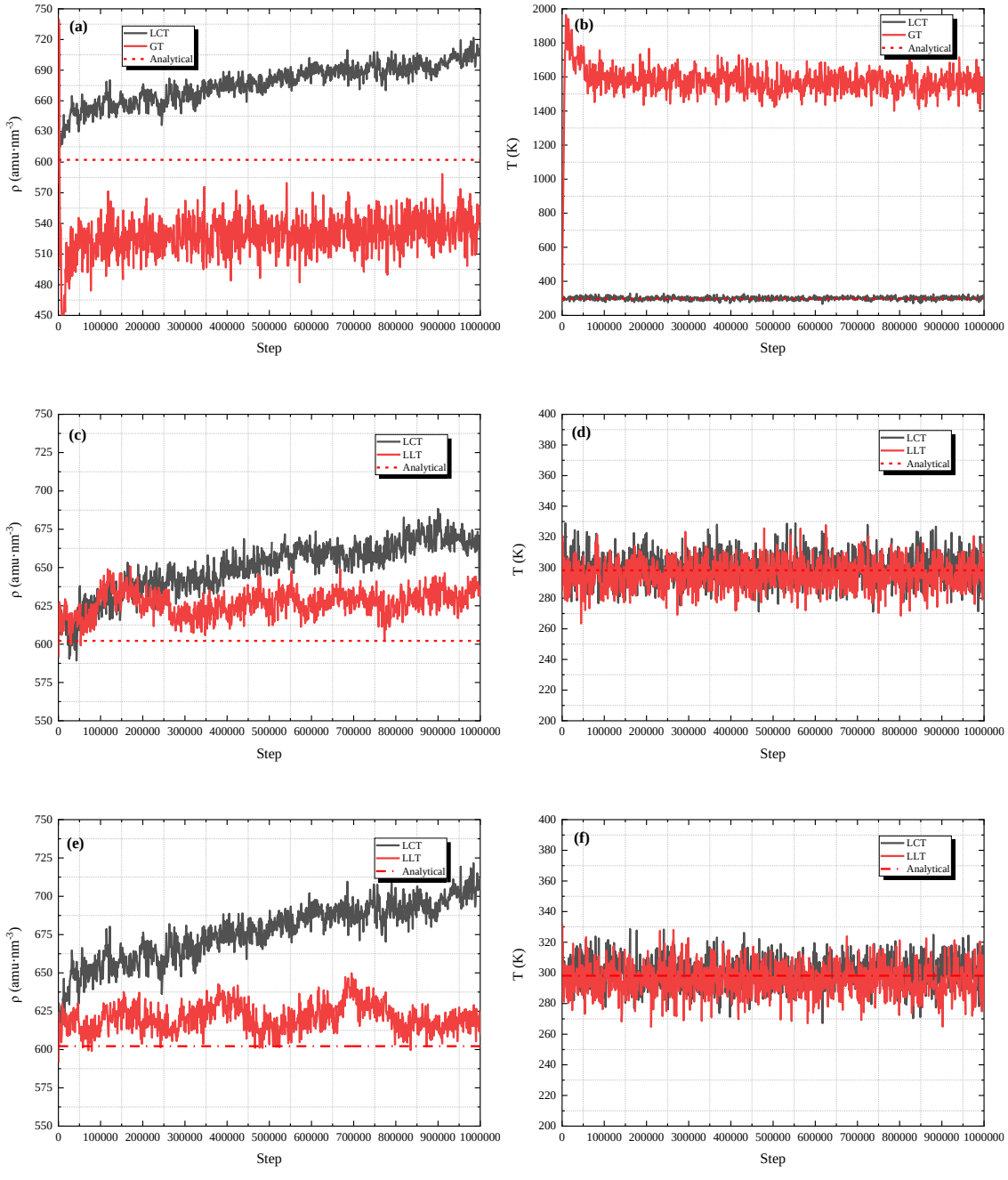

Fig. 2 Fluctuation properties of SPC/E water averaged over the pure MD part of the simulation domain: density fluctuations (a), (c), (e) and temperature fluctuations (b), (d), (f). (a) and (b) correspond to the comparison between the GT and LCT models in the 17×17×17 domain. (c) and (d) correspond to the comparison between the LCT and LLT models in the 9×9×9 domain. (e) and (f) are the same as (c) and (d) but for the 17×17×17 domain. The reference analytical solutions are shown for comparison.

Fig.3 shows distributions of the local temperature of the MD particles across the particle box in the x, y, and z directions for all three models and the two domain sizes. In all cases, the local temperature peaks in the pure MD zone, which corresponds to cell 0 on the plots and then decays to the periphery where the hydrodynamic effects dominate. Notably, both the LCT and the LLT model correctly capture the reference temperature in the pure MD zone.

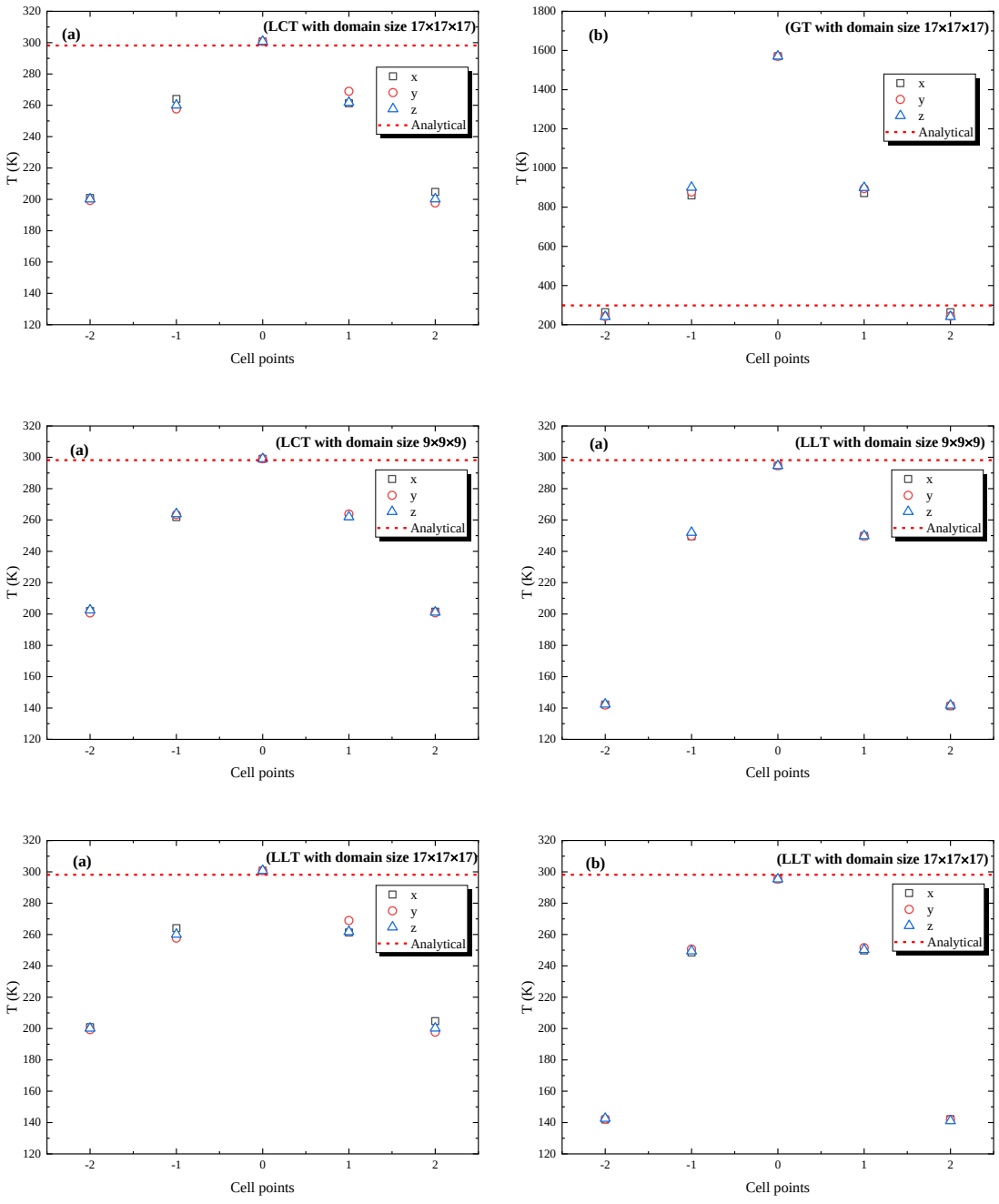

Fig.3 Control volume-averaged temperature distributions across the box simulation domain in the *x*, *y*, and *z* directions for different hybrid models and domain sizes. Cell 0 corresponds to the pure MD region. (a) and (b): LCT and GT results for the domain size 17×17×17. (c) and (d): LCT and

LLT results for the domain size 9×9×9. (e) and (f) are the same as (c) and (d) but for the domain size 17×17×17. The reference temperature is shown by the dashed line.

Finally, Fig.4 shows the radial distribution function (RDF) for O-O atoms produced by the same three models and for the two simulation domain sizes. The reference pure all-atom MD solution is shown on the same plots for comparison. It should be pointed out that RDF directly influences interatomic forces in MD simulations and is one of the critical microscopic distributions which need to be accurately reproduced in atomistic scale-resolving simulations.

Notably, the GT model completely fails to predict the correct distribution which is related to the spurious overheating effect it generates in water. The LCT model correctly captures the first hydration layer but the subsequent dip associated with repulsion is smeared. This is likely due to a notable compression (12% error in the mean density) of the water state this model produces. In comparison with this, the local thermostat based LLT model leads to the most accurate RDF solution which captures well both the first hydration layer and the following repulsion dip of the RDF curve.

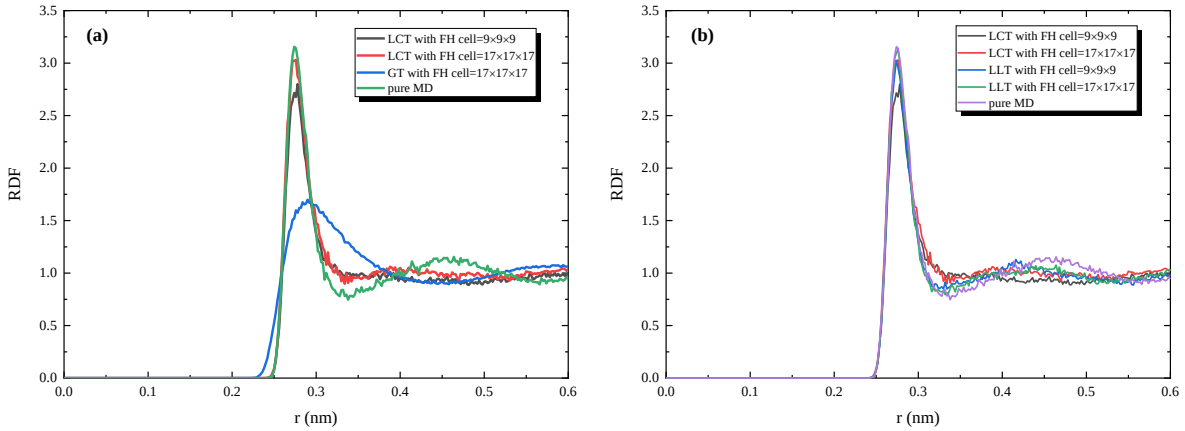

Fig. 4. Radial distribution functions of O-O atoms for different models and simulation domain sizes: GT in the 17×17×17 domain, LCT in the 9×9×9 and 17×17×17 domains, and LLT in the 9×9×9 and 17×17×17 domains. The reference pure all-atom MD solution is included for comparison.

3.3 Computational efficiency

All the three hybrid multiscale models, GT, LCT and LLT correspond to virtually the same computational cost in terms of the number of hours required to calculate the solution for 1 nanosecond simulation time using the same GROMACS version on the same workstation computer. This cost is compared with the computational cost of performing the pure all-atom MD simulations in the same 9×9×9

and 17×17×17 computational domains. The results are summarised in Table 4. Notably, for the smaller computational box, the suggested hybrid models are already about a factor of 5 faster that the pure all-atom MD simulation. Once the simulation domain is increased to 17×17×17, the speed-up factor in comparison with the pure MD method grows to 20. This illustrates potential benefits of using the suggested hybrid methods to significantly reduce the computational time of atomistic-scale simulations of large molecular systems.

Table 4. Simulation costs of the hybrid multiscale methods against the all-atom molecular dynamics for different computational domains, hours per nanosecond (h/ns) in each case.

Simulation size	Small domain (9×9×9)	Large domain (17×17×17)
Cost of the all-atom simulation (h/ns)/cost of the hybrid method (h/ns)	5.93/21.24=0.28	7.54/138.34=0.05

4. Conclusions

A thermostat-consistent hybrid method is developed that fully couples Molecular Dynamics (MD) equations with continuum flow fields. The formulation follows the framework of the Generalised Landau-Lifshitz Fluctuating Hydrodynamics (GLL-FH) method based on the two-phase flow analogy approach for multiscale modelling. The increased consistency is achieved by incorporating the dissipation terms in the governing MD particle equations in accordance with the standard Berendsen thermostat model and subsequently re-deriving the effective source terms of the hydrodynamics part of the model in order to preserve the conservation of mass and momenta. In comparison with the previous MD-FH models based on the same two-phase flow analogy approach[19, 28], which used Global Thermostat (GT) models, the suggested Langevin thermostat-based method does not require any external MD thermostat to keep the simulation stable. A possible extension of the suggested modelling framework to the Nose-Hoover thermostat is also discussed.

Two versions of the new Langevin thermostat-consistent model are implemented: with and without applying a local definition of the reference temperature of the particles depending on the local contribution of the continuum hydrodynamics region in the hybrid simulation domain. These are called Langevin Local Thermostat (LLT) and Langevin Constant Thermostat (LCT) models, respectively. Both the models are implemented in GROMACS for the test problem of SPC/E water fluctuations at equilibrium isothermal conditions based on NVT MD ensemble. The results are compared with those obtained for the same hybrid

method based on the GT model and with the reference pure all-atom MD solutions for different simulation domain sizes.

In contrast to the GT model, the suggested LCT and LLT models are less sensitive to the numerical domain size and reproduce not only correct velocity and density fluctuations but also capture the local temperature in the pure MD region of the computational domain. Furthermore, LLT is also shown to accurately capture the reference water density in the pure MD region, hence, the pressure, which leads to correctly capturing both the first hydration layer and the following repulsion deep of the radial distribution function of water atoms.

All three hybrid models, GT, LCT, and LLT and demonstrate a considerable reduction of the computational cost in comparison with the pure all-atom MD model. Depending on the simulation domain size, the suggested hybrid models are faster by a factor of 5 to 20. This illustrates potential advantages of using the suggested hybrid methods to significantly reduce the computational time of atomistic-scale simulations of large biomolecular systems. Implementation in the popular open-source code such as GROMACS makes the suggested models available to other researchers working in the same area.

Acknowledgement

The work of XL was supported by the China Scholarship Council (CSC). IK and SK gratefully acknowledge the funding under the European Commission Marie Skłodowska-Curie Individual Fellowship Grant No. H2020-MSCA-IF-2015-700276 (HIPPOGRIFFE). The work was also supported by European Commission in the framework of the RISE program, Grant No. H2020-MSCA-RISE-2018-824022-ATM2BT.

References

[1] Zavadlav, J.; Podgornik, R.; Praprotnik, M. *Sci. Rep.* **2017,** *7* (1), 1-11.

[2] Karabasov, S.; Nerukh, D.; Hoekstra, A.; Chopard, B.; Coveney, P. V. *Philos. Trans. R. Soc., A* **2014,** *372* (2021), 20130379.

[3] Borg, M. K.; Lockerby, D. A.; Reese, J. M. *J. Comput. Phys.* **2013,** *233*, 400-413.

[4] Walther, J. H.; Praprotnik, M.; Kotsalis, E. M.; Koumoutsakos, P. *J. Comput. Phys.* **2012,** *231* (7), 2677-2681.

[5] Ren, W.; Weinan, E. *J. Comput. Phys.* **2005,** *204* (1), 1-26.

[6] Yasuda, S.; Yamamoto, R. *Phys. Fluids* **2008,** *20* (11), 113101.

[7] Borg, M. K.; Lockerby, D. A.; Ritos, K.; Reese, J. M. *J. Membr. Sci.* **2018,** *567*, 115-126.
[8] O'Connell, S. T.; Thompson, P. A. *Phys. Rev. E* **1995,** *52* (6), R5792.
[9] Landau, L. D.; Lifshitz, E. M., *Statistical Physics , Part 1*. Elsevier, Amsterdam: 1980; Vol. 5.
[10] De Fabritiis, G.; Delgado-Buscalioni, R.; Coveney, P. *Phys. Rev. Lett.* **2006,** *97* (13), 134501.
[11] De Fabritiis, G.; Serrano, M.; Delgado-Buscalioni, R.; Coveney, P. *Phys. Rev. E* **2007,** *75* (2), 026307.
[12] Voulgarakis, N. K.; Chu, J.-W. *J. Chem. Phys.* **2009,** *130* (13), 04B605.
[13] Flekkøy, E.; Wagner, G.; Feder, J. *EPL (Europhysics Letters)* **2000,** *52* (3), 271.
[14] Delgado-Buscalioni, R.; Coveney, P. *Phys. Rev. E* **2003,** *67* (4), 046704.
[15] Nie, X.; Chen, S.; Robbins, M. *J. Fluid Mech.* **2004,** *500*, 55.
[16] Praprotnik, M.; Delle Site, L.; Kremer, K. *J. Chem. Phys.* **2005,** *123* (22), 224106.
[17] Delgado-Buscalioni, R.; Kremer, K.; Praprotnik, M. *J. Chem. Phys.* **2008,** *128* (11), 114110.
[18] Delle Site, L.; Praprotnik, M.; Bell, J. B.; Klein, R. *Adv. Theory Simul.* **2020,** *3* (5), 1900232.
[19] Markesteijn, A. P.; Karabasov, S. A.; Glotov, V. Y.; Goloviznin, V. M. *Comput. Methods Appl. Mech. Eng.* **2014,** *281*, 29-53.
[20] Pavlov, E.; Taiji, M.; Scukins, A.; Markesteijn, A.; Karabasov, S.; Nerukh, D. *Faraday Discuss.* **2014,** *169*, 285-302.
[21] Korotkin, I.; Nerukh, D.; Tarasova, E.; Farafonov, V.; Karabasov, S. *J. Comput. Sci.* **2016,** *17*, 446-456.
[22] Korotkin, I.; Karabasov, S.; Nerukh, D.; Markesteijn, A.; Scukins, A.; Farafonov, V.; Pavlov, E. *J. Chem. Phys.* **2015,** *143* (1), 014110.
[23] Berendsen, H. J.; van der Spoel, D.; van Drunen, R. *Comput. Phys. Commun.* **1995,** *91* (1-3), 43-56.
[24] Hu, J.; Korotkin, I.; Karabasov, S. *J. Mol. Liq.* **2019,** *280*, 285-297.
[25] Tarasova, E.; Korotkin, I.; Farafonov, V.; Karabasov, S.; Nerukh, D. *J. Mol. Liq.* **2017,** *245*, 109-114.
[26] Li, F.; Korotkin, I.; Taiji, M.; Karabasov, S. **2020,** *DOI: 10.13140/RG.2.2.14247.57763*.
[27] Hu, J.; Korotkin, I.; Karabasov, S. *J. Chem. Phys.* **2018,** *149* (8), 084108.
[28] Korotkin, I.; Karabasov, S. *J. Chem. Phys.* **2018,** *149* (24), 244101.
[29] Scukins, A.; Nerukh, D.; Pavlov, E.; Karabasov, S.; Markesteijn, A. *Eur. Phys. J.: Spec. Top.* **2015,** *224* (12), 2217-2238.
[30] Buckley, S. E.; Leverett, M. *Trans. AIME* **1942,** *146* (01), 107-116.
[31] Van Gunsteren, W. F.; Berendsen, H. J. *Mol. Simul.* **1988,** *1* (3), 173-185.
[32] Berendsen, H. J.; Postma, J. v.; van Gunsteren, W. F.; DiNola, A.; Haak, J. R. *J. Chem. Phys.* **1984,** *81* (8), 3684-3690.
[33] Passler, P. P.; Hofer, T. S. *J. Comput. Chem.* **2017,** *38* (5), 265-275.
[34] Qu, S.; Shastry, V.; Curtin, W.; Miller, R. E. *Modell. Simul. Mater. Sci. Eng.* **2005,** *13* (7), 1101.
[35] Nosé, S. *J. Chem. Phys.* **1984,** *81* (1), 511-519.

Appendix A: Effect of the shape function $f(s)$ on the local thermostat model

To illustrate the effect of the shape function, three types of functions have been tested, $f(s)=\sqrt{(1-s)}$, $f(s)=(1-s/2)$, and $f(s)=(1-s)^{-1}$. In comparison with the first two choices, the third option, $f(s)=(1-s)^{-1}$ does not satisfy Eq.(29). Fig. A1, shows the resulting ensemble-averaged temperature time history in the pure molecular dynamics zone of the hybrid simulation domain. Both $f(s)=\sqrt{(1-s)}$ and $f(s)=(1-s/2)$ lead to satisfactory temperature fluctuations around the target reference temperature. In contrast to this, the choice of $f(s)=(1-s)^{-1}$ leads to a lower temperature and larger fluctuations in the centre of the simulation domain thereby resulting in the model divergence before reaching the target time step (10^6).

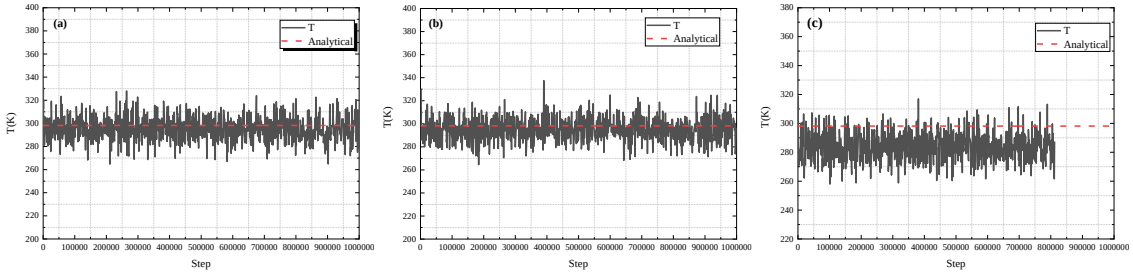

Fig.A1. Temperature fluctuations for different shape functions: (a) $f(s)=(1-s/2)$ (b) $f(s)=\sqrt{(1-s)}$, and (c) $f(s)=(1-s)^{-1}$.